Validation of Added Resistance Computations by a Potential-Flow Boundary-Element Method

Joncquez, Soizic Annick Gabrielle; Bingham, Harry B.; Andersen, Poul; Kring, David

Published in:
Proceedings of the 27th Symposium on Naval Hydrodynamics

Publication date:
2008

Document Version
Early version, also known as pre-print

27th Symposium on Naval Hydrodynamics
Seoul, Korea, 5-10 October 2008

Validation of Added Resistance Computations by a Potential-Flow Boundary-Element Method

Soizic A. G. Joncquez, Harry Bingham, Poul Andersen
(Technical University of Denmark, Denmark)
David Kring (Flight Safety Technology, USA)

ABSTRACT

Second-order forces have been widely investigated using 2D methods and more recently, also using 3D methods. The present work uses the 3D, time-domain, high-order boundary element code AEGIR to calculate the second order forces. Results for added resistance using both pressure integration and conservation-of-momentum methods are presented and compared with published data and experimental measurements. The two methods give consistent results for simple geometries like a sphere and the Wigley hull. More complex geometries such as the Series 60 hull and a bulk carrier are also calculated but only with the momentum conservation method. The results demonstrate the accuracy and flexibility of this method which is not overly sensitive to the details of the geometry.

INTRODUCTION

The robust prediction of added resistance in a seaway is of importance to both commercial and naval ships since it affects both economic performance and operational range. In order to provide guidance on added resistance to designers at an early stage, it has been necessary to develop efficient computational tools. In the 70's and 80's, many methods based on strip theory were proposed including Gerritsma and Beukelman (1972), Salvesen (1978) and Faltinsen (1980). However, these methods have some limitations such as the assumption of wall-sided ships (vertical section shapes at the waterline). This limitation is restrictive as most ships will have some degree of flare. Moreover these two methods do not take into account wave diffraction, which is the main component of the added resistance for short waves. Faltinsen's method, which does account for diffraction, is only valid for short waves.

In order to address these limitations a 3D method is required that can take into account the most significant effects. One of the tools available for a designer is the seakeeping code AEGIR. It considers zero-speed, slow and fast ships, and incorporates linear and nonlinear formulations. Previous work from Kring (2004) has shown the accuracy and validity of the results and AEGIR's wide geometric flexibility. AEGIR can compute steady resistance and motions in waves for multiple hulls, multiple bodies, offshore platforms, conventional and advanced ships with lifting bodies. Its advanced NURBS based geometry engine provides an essentially exact geometric representation of the CAD design with automatic waterline intersection during the simulation.

The purpose of this paper is to present two methods widely used to calculate second-order forces, which have been implemented in AEGIR: the pressure integration method and the momentum conservation method. The results obtained are compared with experimental data and previously published calculations for four different geometries: a sphere, a Wigley hull, a Series 60 and a bulk carrier. Good agreement is found by the pressure integration method for the half submerged sphere. The momentum conservation method also gives good results for the Series 60, the Wigley hull and the bulk carrier. However, for the latter geometry AEGIR slightly underestimates the added resistance compared to the experimental results.

THE BOUNDARY VALUE PROBLEM

A floating body moving with forward velocity, through an incompressible ideal fluid is considered. Two frames are used: the first one (x_0, y_0, z_0) is a fixed inertial frame and the second one (x, y, z) is a reference frame fixed with respect to the steady motion of the ship.

The reference frame is translating in relation to the inertial frame with a mean forward speed U and the mean slide-slip speed V and is rotating with the mean rotation Ω. The surface S_F represents the free surface. The surface S_B represents the instantaneous submerged hull surface.

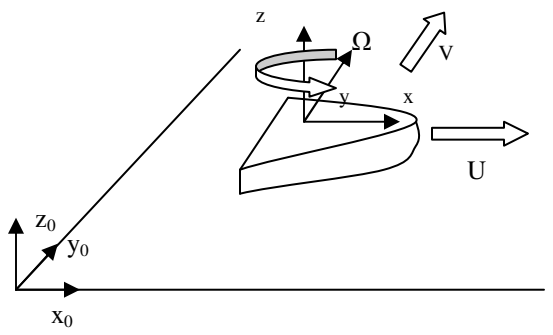

Figure 1: Representation of the two frames

The mean velocity field $\vec{W}$ is defined as:

$$\vec{W} = (U - \Omega y)\vec{i} + (V + \Omega x)\vec{j} \tag{1}$$

$(\vec{i}, \vec{j}, \vec{k})$ representing the unit vectors associated with the fixed frame.
The Boundary Value Problem is expressed with respect to the reference frame $\vec{x}$. The fluid is assumed to be inviscid and incompressible and the the flow is irrotational. The potential function is represented by $\Psi(\vec{x},t)$. It satisfies mass conservation (the Laplace equation) in the fluid domain:

$$\nabla^2\Psi(\vec{x},t) = 0 \tag{2}$$

Bernoulli's equation relates the pressure to the potential function in the inertial frame. The general expression is:

$$p - p_a = -\rho\left(\frac{d\Psi}{dt} + \frac{1}{2}\nabla\Psi\cdot\nabla\Psi + gz\right) \tag{3}$$

The Galilean transformation is used in order to express the equation (3) in the moving reference frame.

$$\frac{d}{dt} = \frac{\partial}{\partial t} - \vec{W}\cdot\nabla \tag{4}$$

This means that the Bernoulli equation in the moving reference frame is expressed as:

$$p - p_a = -\rho\left(\frac{\partial\Psi}{\partial t} - \vec{W}\cdot\nabla\Psi + \frac{1}{2}\nabla\Psi\cdot\nabla\Psi + gz\right) \tag{5}$$

A "no-flux" condition is imposed on the submerged body B. This is expressed as:

$$\frac{\partial\Psi}{\partial n} = \vec{V}_B\cdot\vec{n} \qquad \text{on} \quad S_B \tag{6}$$

$\vec{V}_B$ represents the total fluid velocity on the hull surface. The domain is also bounded by the free surface. Wave overturning is not allowed. The free surface elevation $\varsigma(x,y,t)$ follows the kinematic free-surface boundary condition in the reference frame:

$$\left(\frac{\partial}{\partial t} - \left(\vec{W} - \nabla\Psi\right)\cdot\nabla\right)\left(z - \zeta(x,y,t)\right) = 0$$
$$\text{on} \quad z = \varsigma(x,y,t) \tag{7}$$

The dynamic free-surface boundary condition states that the pressure on the free surface must be equal to the atmospheric pressure. Through the Bernoulli equation the following expression is obtained:

$$\varsigma(x,y,t) = -\frac{1}{g}\left[\frac{\partial\Psi}{\partial t} - \vec{W}\cdot\nabla\Psi + \frac{1}{2}\nabla\Psi\cdot\nabla\Psi\right]$$
$$\text{on} \quad z = \varsigma(x,y,t) \tag{8}$$

The final condition to close the boundary value problem is the wave radiation condition. A numerical beach that utilizes Newtonian cooling and dispersion compensating Rayleigh viscosity modify the free-surface condition in an outer zone that absorbs outgoing waves.

The total potential $\Psi(\vec{x},t)$ is linearized up to order 2 with respect to the steady base flow Φ.

$$\Psi = \Phi + \phi^1 + \phi^2 \tag{9}$$

In AEGIR the steady base flow can be developed from the Neumann-Kelvin linearization (free stream), double-body flow, or from a fully nonlinear steady state wave solution. The present work only considers the Neumann-Kelvin linearization.

The boundary value problem formulated above allows for the solution of the wave radiation and diffraction for a ship moving in a seaway based on a mixed numerical scheme. The balance of explicit temporal integration for the kinematic, implicit integration for the dynamic free-surface boundary condition, and a high-order boundary element

solution of the governing equations provides for a stable solution of the wave flow with no numerical dispersion. Given the wave forces and resulting first-order forces, the motion of the ship is computed at each time step using a 4th-order Runge-Kutta integration. Care is taken to treat the zero-frequency added mass term implicitly within the equation of motion.

After computing this underlying solution for the wave flow and the body motion, two general methods have been developed to calculate the second-order forces and moments: the pressure integration method and the momentum conservation method. Both are presented in the following sections.

Pressure Integration Method

The pressure integration method is the most widely used to calculate the second order forces. The normals n_i represent the general normals:

n_i , i = 1,3 the normals in the x, y and z directions

n_i , i = 4,6 the vector $\vec{x} \times \vec{n}$

According to the theory, the instantaneous forces can be expressed as:

$$F_i = \int_{S_B} p n_i ds \qquad \text{i=1,6} \tag{10}$$

Where F_i with i=1, 3 represents the forces and F_i with i=4, 6 the moments. As shown on figure 2, the instantaneous wetted surface of the hull can be divided into three surfaces:

1. The mean wetted surface in calm water
2. The surface coming from the pitching/heaving of the ship
3. The surface coming from the incoming waves

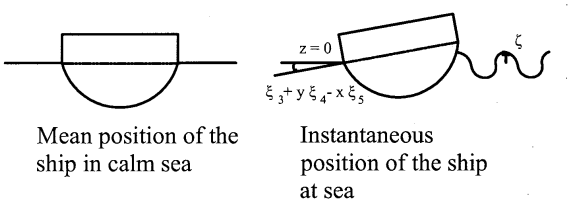

Figure 2: Instantaneous surface of the hull

The integrals over the two latter surfaces are a combination of integrals over the waterline and the vertical component of the surface of the ship along t_z. Figure 3 shows the link between the coordinate z and the coordinate t_z. It is assumed that the heave, the roll and the pitch motions are small compared to the principal dimensions of the ship. Therefore the relative flare angle α is assumed to be independent of z.

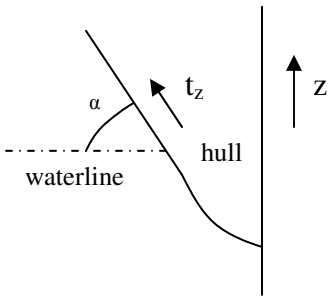

Figure 3: Link between local and global frames.

The expression of the generalized forces is:

$$F_i = \int_{S_{\bar{B}}} p n_i ds + \iint_{wl} \int_{\xi_3 + y\xi_4 - x\xi_5}^{0} p \frac{n_i}{\sin\alpha} dz dl + \iint_{wl} \int_{0}^{\zeta} p \frac{n_i}{\sin\alpha} dz dl \tag{11}$$

ξ_3, ξ_4 and ξ_5 represent the heave, the roll and the pitch. α is the flare angle of the hull measured at z=0. The first integral is due to the pressure on the mean position of the body, whereas the second and third integral take into account the motion and the wave elevation.

The second-order generalized force only comes from the integral of the second order pressure on the mean body. According to equation (5) the generalised forces $F^{mb}{}_i$ can be expressed as:

$$F^{mb}{}_i = \int_{S_{\bar{B}}} p^{(2)} n_i ds \tag{12}$$

$$p^{(2)} = -\rho \left[\frac{\partial \phi^{(2)}}{\partial t} + \left(-\vec{W} + \nabla\Phi \right) \cdot \nabla \phi^{(2)} + \frac{1}{2} \nabla \phi^{(1)} \cdot \nabla \phi^{(1)} \right] - \rho X \cdot \nabla \left[\frac{\partial \phi^{(1)}}{\partial t} + \left(-\vec{W} + \nabla\Phi \right) \cdot \nabla \phi^{(1)} \right]$$

where X represents the motion of the point. The second-order pressure is derived from the sum of

second-order potential in the Bernouilli equation and the interaction between the ship motion and the gradient of the first-order pressure.

In this paper, the second-order potential is neglected since it will not contribute to the mean second-order added resistance or drift forces and moments. For the integrals considering the wave elevation and the motion of the ship, the second-order forces F_{wl} will come from the first-order pressure, as the motions and the wave elevations are quantities of first order. The first-order pressure is obtained by applying a Taylor expansion to equation (5). Using the linear assumptions, the final expressions for the forces Fwl are:

$$\vec{F}_{wl} = \frac{1}{2}\rho g \int_{wl} \left[(\varsigma - \xi_3 - y\xi_4 + x\xi_5)^2\right]\vec{n}dl \tag{13}$$

Momentum Conservation Method

The other method widely used to calculate the second order forces is based on the conservation of the momentum. The momentum $\vec{M}(t)$ can be expressed as:

$$\vec{M}(t) = \iiint_{\Omega} \rho\vec{V}d\tau \tag{14}$$

Ω is the volume defined by the instantaneous wetted surface of the hull S_B, the instantaneous free surface S_F and a control surface (a cylinder) very far away from the hull, as shown on Figure 4.

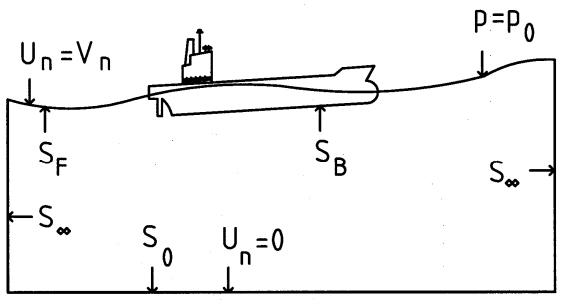

Figure 4: Representation of the control volume Ω

Both velocity and volume change with time.

$$\frac{d\vec{M}}{dt} = \iiint_{\Omega} \rho\frac{d\vec{V}}{dt}d\tau + \iint_{S} \rho\vec{V}U_n ds \tag{15}$$

By use of the Galilean transformation and the Euler equation, the expression of the change in momentum can be simplified to

$$\frac{d\vec{M}}{dt} = \iiint_{\Omega} -\nabla(p+\rho gz)d\tau - \iiint_{\Omega}\vec{V}\cdot\nabla\vec{V}d\tau + \iint_{S}\rho\vec{V}U_n ds \tag{16}$$

The term $\nabla(\rho gz)$ is dropped as only the horizontal forces and moments are calculated in this study. This assumption, along with Green's First Identity leads to the following simplified expression for equation (16).

$$\frac{d\vec{M}}{dt} = -\rho\iint_{S}\left[\frac{p}{\rho}\vec{n} - \vec{V}(V_n - U_n)\right]ds \tag{17}$$

S can be divided into four surfaces: a surface at infinity S_∞, the free surface S_F, the wetted hull surface S_B and the surface at the bottom S_0. The surface S_∞ is a cylinder. $U_n=V_n$ on S_F and S_B but $U_n=0$ on S_0 and S_∞. The pressure is constant on S_0 and zero on S_F. With these properties, the equation of the momentum change can be simplified to:

$$\frac{d\vec{M}}{dt} = -\rho\iint_{S_B}\frac{p}{\rho}\vec{n}ds - \rho\iint_{S_\infty}\left[\frac{p}{\rho}\vec{n} + \vec{V}V_n\right]ds \tag{18}$$

By use of the conservation of momentum, the mean horizontal forces are then equal to:

$$\bar{\vec{F}} = -\rho\iint_{S_\infty}\left[\frac{p}{\rho}\vec{n} + \vec{V}V_n\right]ds \tag{19}$$

S_d is the part of S_∞ lying below z=0 and C_d is the intersection of S_∞ with the z=0 plane. The linear formulation is used and the final expression for the second order horizontal forces is:

$$\bar{\vec{F}} = -\rho\iint_{S_d}\left[-\frac{g}{2}(\nabla\phi\cdot\nabla\phi)\vec{n} + \vec{V}V_n\right]ds - \frac{\rho g}{2}\int_{C_d}\varsigma^2\vec{n}dl \tag{20}$$

EXPERIMENTAL DESCRIPTION

The program has been tested with a bulk carrier shown in figure 5. The main dimensions are indicated in table 1.

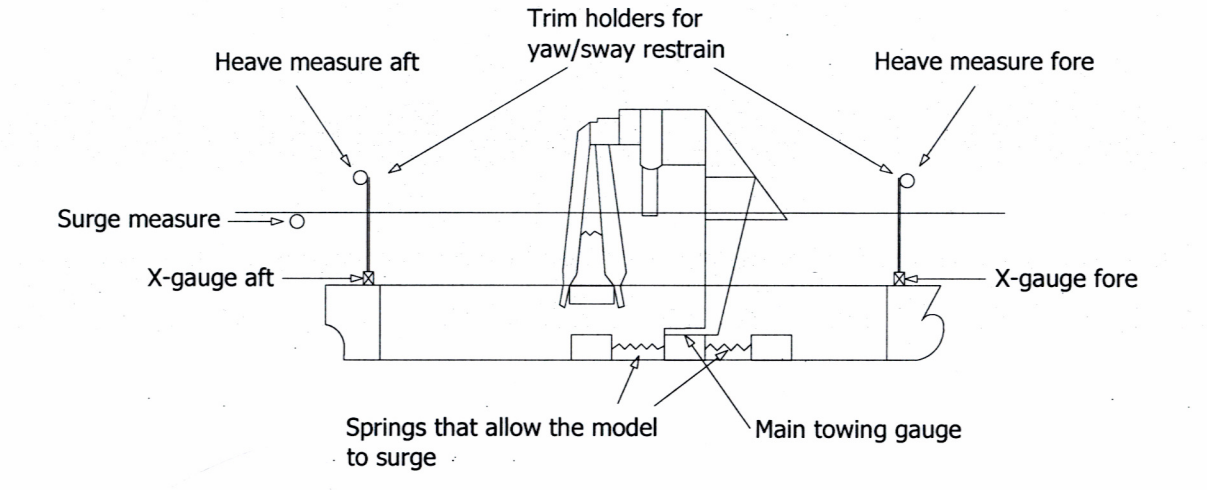

Figure 6: Representation of the setup of the experiment for the bulk carrier

Table 1: Main dimensions of the bulk carrier

Length	L	m	183.25
Breadth	B	m	32.2
Draught	T	m	11.1
Trim	t	m	0.0000
Volume of displacement	∇	m^3	54922
Block coefficient	C_B	-	0.814

Experimental values were obtained at FORCE Technology, Denmark. During the experiment, the model was free to surge, heave and pitch. The heave and surge motions were measured. Figure 6 shows the setup used. A special feature of the setup is the inclusion of the surge motion by means of two springs. The surge motion has a small influence on the added resistance coefficient.
During the experiment, the accuracy of the wave period is high, but it was difficult to obtain precise wave amplitudes.

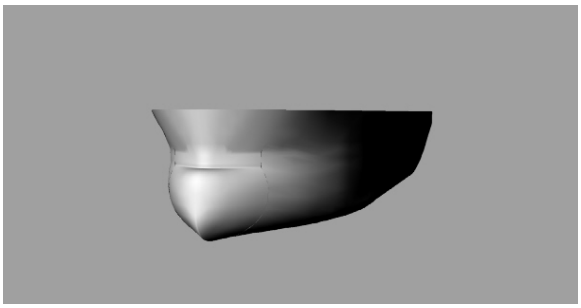

Figure 5: Perspective view of the bulk carrier

For each wave series, three possible amplitudes can be used: the RMS-amplitude, the minimum amplitude and the maximum amplitude. The minimum amplitude is the lowest amplitude on the time record and the maximum amplitude is the highest. Figure 7 shows the three amplitudes for different dimensionless frequencies of encounter μ_e for 14 knots.

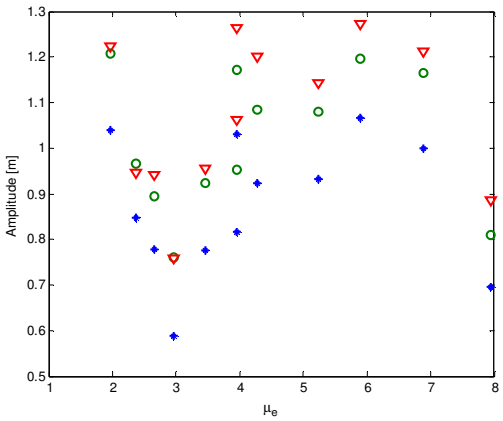

Figure 7: Value of the RMS-amplitude, the minimum amplitude and the maximum amplitude for different frequency of encounter, for 14 knots. Blue star: Arms. Green circle: Amin. Red triangle: Amax.

Figure 7 reveals that the minimum and maximum amplitude are usually quite closed. On the other hand the RMS –amplitude, which is supposed to be the most accurate, appears to be quite different from the

two other amplitudes. Figure 7 also shows how much the wave amplitude is varying.

RESULTS AND DISCUSSION

Four different floating bodies are considered: a half-submerged sphere, a Wigley hull, a Series 60 and a bulk carrier. The main data of the Wigley hull and the Series 60 are represented in table 2 and 3. The half-submerged sphere and the Wigley hull are used as tests case for respectively the pressure integration method and the momentum conservation method.

The Froude number is defined as $U/\sqrt{gL}$, U and L corresponding respectively to the forward speed and the significant length. For the sphere, L is the radius *a* and for the Wigley hull, the Series 60 and the bulk carrier L is the length between perpendiculars. Only head seas are considered.

Fixed half-submerged sphere, low forward speed

The added resistance coefficient σ_{aw} is made dimensionless for the sphere by dividing by $\rho g A^2 a$. A denotes the amplitude of the wave. The pressure integration method is used by AEGIR. Figure 8 shows the added resistance coefficient from AEGIR and Grue (1993). The sphere is restrained in motion. The two sets of data seem to be quite different. However this difference could come from the difference in the method. Grue (ibid) used a linearization with respect to the forward speed, which is not the case of the present method. Moreover, Grue (ibid)'s method is based on momentum conservation.

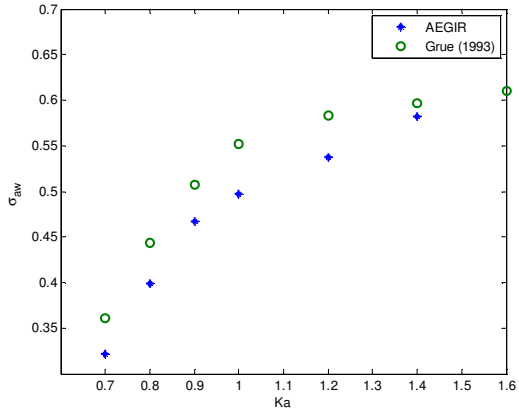

Figure 8: Mean drift force for a half-submerged sphere at Fn = 0.04. K is the wavenumber and a is the radius of the sphere.

Half-submerged sphere, no forward speed

The sphere is free to move in surge and heave. There is no forward speed. The sphere and the free surface are illustrated in figure 9.

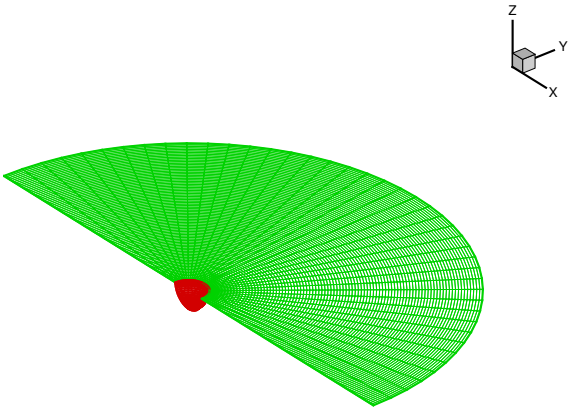

Figure 9: Representation of the free surface for the half submerged sphere

Figure 10 shows the added resistance coefficient from AEGIR, Choi et al (2000) and Kudoh (1977). Kudoh's results are analytical. AEGIR is giving results that are very close to the results given by Choi (ibid). The highest relative difference is 2%, which is located at the resonance, Ka=1.2.

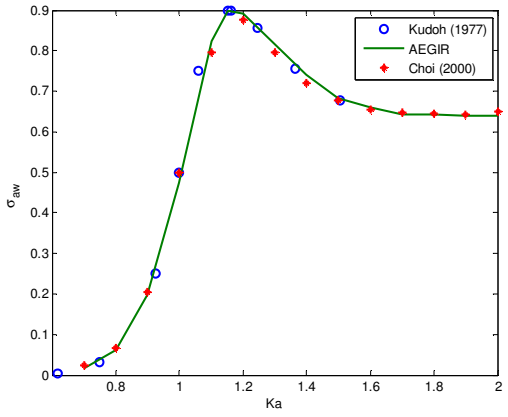

Figure 10: Mean drift force for a half submerged sphere, Fn=0.

In AEGIR's current configuration, the momentum conservation method can not be used for the sphere case which needs to use a circular free-surface shape.

The panel arrangement in this case prevented good numerical convergence for the momentum conservation method since the panels expanded in the far-field. This could be corrected in the future by adding the capability to handle multiple internal knots of the free surface which would allow a more flexible discretization.

The Wigley hull I

The Wigley hull will be used as a first test of the momentum conservation method. Also, moving away from the sphere, added resistance will now be non-dimensionalized by $\rho g A^2 B^2/L$, where B denotes the breadth of the ship. The Wigley hull chosen corresponds to the Wigley hull I in Journées (1992).

Table 2: Main dimensions of the Wigley hull I

Length	L	m	3.0000
Breadth	B	m	0.3000
Draught	T	m	0.1875
Trim	t	m	0.0000
Volume of displacement	∇	m^3	0.0946
Center of rotation above base	KR	m	0.1875
Center of gravity above base	KG	m	0.1700
Radius of inertia for pitch	k_{yy}	m	0.7500
Amidships section coefficient	C_m	-	0.9090
Length to breadth ratio	L/B	-	10

The Wigley hull is free to heave and pitch. Figures 11(a), 11(b) and 11(c) show respectively the heave and pitch motions and the added resistance for Fn = 0.3. At low wavelength, the heave predicted by AEGIR is slightly lower than the heave measured during the experiment. However the heave predicted around the peak is higher than the heave measured. At long wavelengths, both predicted and measured heave are close.

The pitch motion has a discrepancy at high wavelength. It can be noticed that the heave and the pitch are well estimated in different regions.

From the figure 11(c), it can be seen that there is a good agreement between the predicted added resistance and the measured one, even at the peak. This means that the difference noticed for the heave motion at the peak does not have any influence on the final results for the added resistance. This also means that the results predicted by AEGIR are more realistic as the maximum added resistance coefficient should happen at the heave resonance, which is not the case for the experimental data.

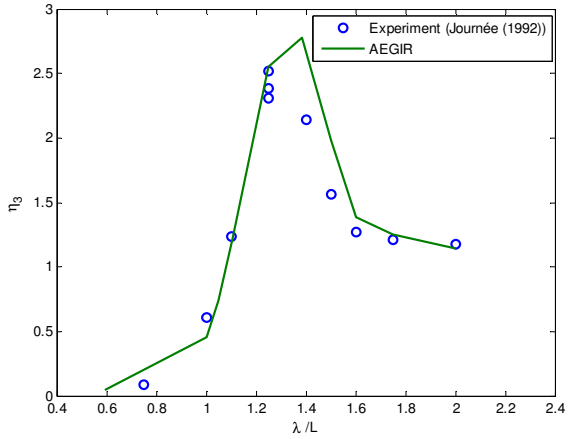

(a)

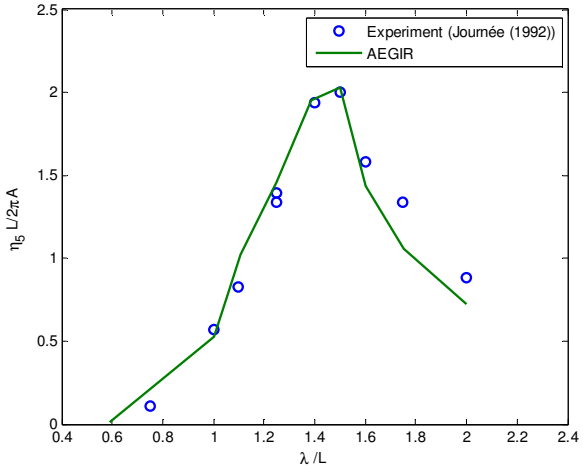

(b)

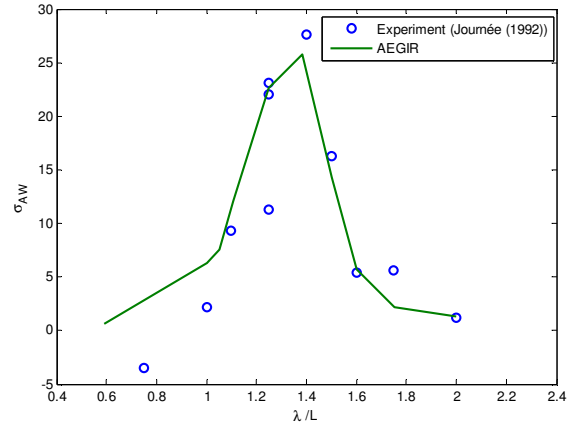

(c)

Figure 11: (a) Heave motion for the Wigley hull I, Fn=0.3. (b) Pitch motion for the Wigley hull I, Fn=0.3. (c) Mean added resistance coefficient for the Wigley hull I, Fn=0.3. λ represents the wavelength.

For short waves the added resistance is slightly higher from AEGIR. However, it can be noticed that some of the experimental values measured for these short waves give negative added resistance which seems unphysical. This negative resistance combined with the evident scatter in the experimental values demonstrates that added resistance is a difficult quantity to obtain experimentally.

The Series 60

The added resistance was computed for the Series 60 and compared with experimental values from Strom-Tejsen (1981) for two speeds: Fn=0.207 and Fn=0.222. Results for momentum conservation are presented. The ship was free to heave and pitch. μ_e is the dimensionless frequency of encounter and is defined as

$$\mu_e = \omega\sqrt{\frac{L}{g}} \qquad (21)$$

ω is the frequency of encounter.

Table 3: Main dimensions of the series 60

Length	L	m	3.0000
Breadth	B	m	0.4284
Draught	T	m	0.1710
Trim	t	m	0.0000
Volume of displacement	∇	m^3	0.1538
Radius of inertia for pitch	k_{yy}	m	0.7500
Block coefficient	C_B	-	0.7
Length to breadth ratio	L/B	-	7

The Series 60 is presented in figure 12.

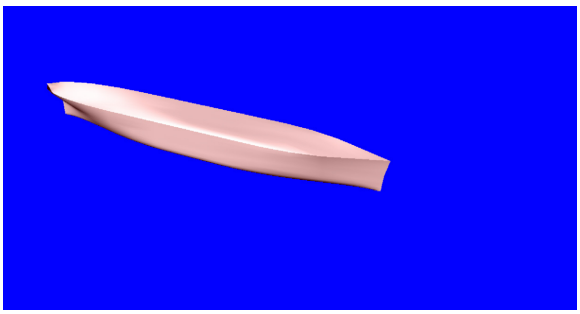

Figure 12: View of the Series 60, the view is from the top left side.

Figures 13 and 14 reveal that AEGIR generally predicts the added resistance coefficient well. However for both speeds a little shift of the peak is noticed. For both cases, the added resistance is overestimated for long waves. It is quite surprising to see that the estimation of the added resistance for short waves is so different between the two speeds. For the lowest speed, it is well estimated whereas for the highest speed there is a factor 2 between experimental values and predictions. But there is quite a difference between the experimental added resistance for Fn = 0.207 and Fn = 0.222 even if the speed is not so different.

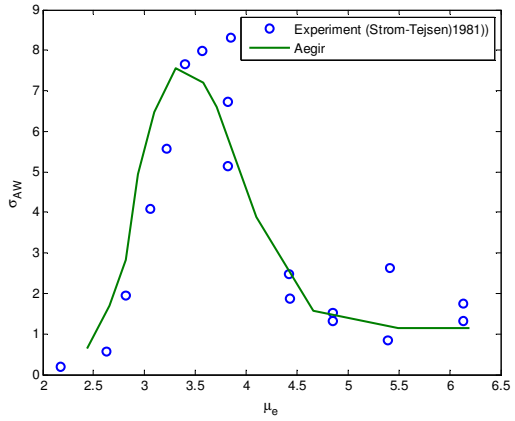

Figure 13: Added resistance coefficient for the Series 60, Fn=0.207

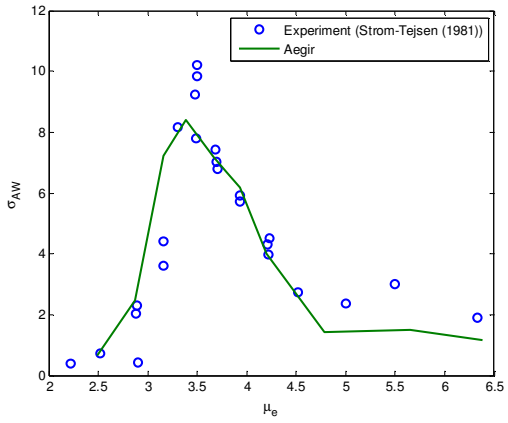

Figure 14: Added Resistance coefficient for the Series 60, Fn = 0.222.

The Bulk Carrier

The last test case studied is the bulk carrier whose main dimensions are found in table 1. The results obtained by Aegir are compared with results obtained with three strip theory methods: Gerritsma and Beukelman (1972), Salvesen (1975) and Faltinsen

(1980). The experimental results are presented as data points with error bars. Figure 15 represents the added resistance coefficient calculated by the three different amplitudes presented previously.

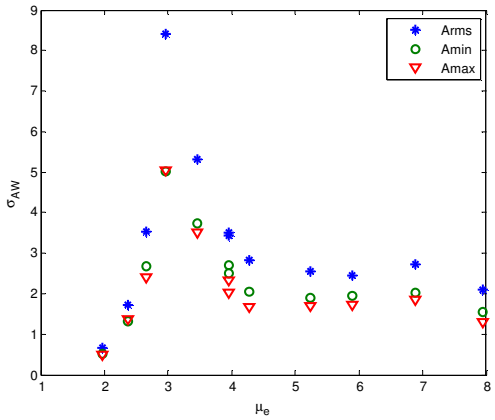

Figure 15: Value of the added resistance coefficient depending on the RMS amplitude, the minimum amplitude and the maximum amplitude.

Figure 15 expresses how the amplitude considered for the normalization can have a high impact on the final value of the added resistance coefficient highest impact is around the "peak". This is quite a delicate part as it corresponds to the heave resonance of the ship.

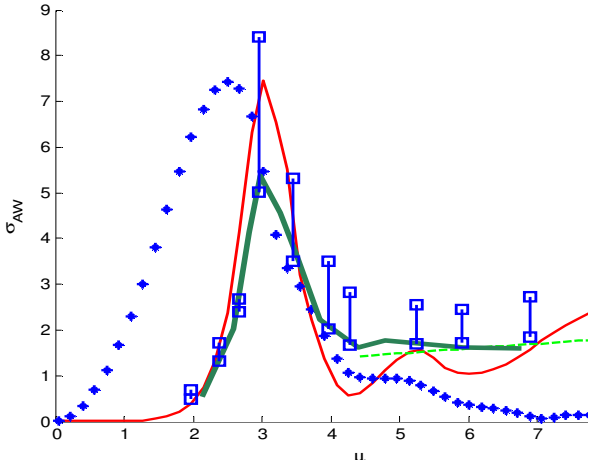

Figure 16: Comparison of the added resistance coefficient predicted by various strip theory method, by AEGIR and measured during the experiment, Speed=14 knots. Blue stars: Salvesen's method (1975), Red plain line: Gerritsma and Beukelman's method (1972), Dashed green line: Faltinsen's method (1980). Plain blue line with square: Experiment with error bars.Plain green line: AEGIR

Figure 16 collects the measured data with error bars determined by the three amplitudes and compares them with computations.

Results of various numerical methods as well as experimental results are shown in figure 16. AEGIR results follow the shape of the experimental curve but underpredict the mean value. In fact AEGIR's results seem to agree quite well with the minimum and maximum amplitude values. This may indicate an irregularity in the RMS calculation for the experiment.

Results from Salvesen's (1975) method are not fitting well the experimental data: it seems that there is a shift in all the values obtained. Faltinsen's (1980) method is fairly accurate in its range of application. Faltinsen also discuss his method in one of his book (1990). A dominant effect on this curve might come from the shape of the bulb: the bulb is fat and flat and may be creating lot of added resistance. Gerritsma and Beukelman's (1972) method is the 2D method that fits the experiments best. However the predicted added resistance rises as the waves get shorter.

As a conclusion Gerritsma and Beukelman's method (1972) may better estimate the peak if the RMS calculation is accurate but at short waves, results are getting worse. AEGIR and the momentum conservation method is a reliable tool to estimate the added resistance coefficient and includes important 3D effects. AEGIR can be trusted for the entire range of frequencies.

CONCLUSION

The momentum conservation method was tested for the Wigley hull, the Series 60 and a bulk carrier. In each case, it was giving results in good agreement with experimental data.

Results from bulk carrier are of interest as they show that the present method is giving fair results for full form ships.

The results presented in this paper were obtained with the Neumann-Kelvin linearization. The next step of the research would be to compare the experimental results with results from the momentum conservation with double-body flow linearization.

ACKNOWLEDGEMENT

Thanks are due to Force Technology for sponsoring the experiments for the bulk carrier.
Thanks are also due to Carl Bro A/S for permission to use one of their bulk carrier design to make tests.
Finally thanks to Benjamin Pedersen for helping doing the experiment and his advice on the results obtained.

REFERENCES

Aanesland, A., "A Hybrid Model for Calculating Wave-Making Resistance", 5th International Conference on Numerical Ship Hydrodynamics, 1990.

Bertram, V., Yasukawa, H., Berthome,M. and Tvergaard, T., " Added Resistance for a fully three-Dimensional Ship Seakeeping Method", 2nd Numerical Towing Tank Symposium, Rome, August 1999

Choi, Y.C., Hong, S.Y., and Choi, H.S.,"An Analysis of Second-order Wave Forces on Floating Bodies by Using Higher-Order Boundary Element Method", Ocean Engineering, Vol. 28, 2000, pp 117-138.

Faltinsen, O. M., Sea Loads on Ships and Offshore Structures, Cambridge University Press, 1990.

Fang, M., and Chen, G., "On the nonlinear hydrodynamic forces for a ship advancing in waves", Ocean Engineering, Vol. 3, 2006.

Gerritsma, J., and Beukelman, W., "Analysis of the resistance increase in waves of a fast cargo ship", International Shipbuilding Progress, Vol. 19, pp. 285-293, 1972

Grue, J., and Biberg, D.,"Wave Forces on Marine Structures with Small Speed in Water of Restricted Depth", Applied Ocean Research, Vol. 15, 1993, pp. 121-135.

Journée, J. M. J, "Experiments and Calculations on Four Wigley Hull Forms in Head Waves", 0909, May 1992, Delft University of Technology.

Kring, D. C., Milewski, W. M. and Fine, N. E.,"Validation of a NURBS-Based BEM for Multihull Ship Seakeeping", 25th Symposium on Naval Hydrodynamics, 8-13 August 2004.

Kudoh, K., "The drifting force acting on a three-dimensional body in waves", Journal of Society of Naval Architects in Japan. Vol 141, pp. 71-77, 1977

Liapis, N., Skjørdal, S. O., Faltinsen, O. M., Minsaas, K. J., "Prediction of resistance and propulsion of a ship in a seaway", Proceedings of the 13th Symposium on Naval Hydrodynamics, 1980.

Nakos, D. E., and Sclavounos, P. D., "Kelvin Wakes and Wave Resistance Cruiser- and Transom-Stern Ship", Journal of Ship Research,, Vol. 38, pp. 9-29, March 1994.

Newman, J. N., "The Drift Force and Moment on Ships in Waves", Journal of Ship Research, 1967

Newman, J. N., "The Second-Order Slowing Varying Force and Moment on a Submerged Slender Body advancing beneath an irregular Wave system", 1973, unpublished

Newman, J. N., "Second-Order Diffraction in Short Waves", Journal of Ship Research, December 2005

Salvesen, N., "Second-Order Steady-State Forces and Moments on Surface Ships in Oblique regular Waves", The Dynamics of Marine Vehicles and Structures in Waves, pp. 212-226, 1975

Strom-Tejsen, J., Yeh, H. Y. H., and Moran, D. D., "Added Resistance in Waves", Transaction of SNAME, pp. 109-143, 1981